Weak turbulent behavior and dynamical frequency locking in a high-Fresnel-number laser

Víctor M. Pérez-García
Departamento de Física Teórica I, Facultad de Ciencias Físicas, Universidad Complutense, Ciudad Universitaria s/n, E-28040 Madrid, Spain

J.M. Guerra
Departamento de Óptica, Facultad de Ciencias Físicas, Universidad Complutense, Ciudad Universitaria s/n, E-28040 Madrid, Spain

(Received 2 April 1993; revised manuscript received 12 November 1993)

A correlation experiment together with previous experimental information supports the existence of a very disordered state in a high-Fresnel-number dye laser that was studied. All the experimental evidence points out that the disordered state can be identified with weak turbulence, allowing for the description of real turbulence (not only *chaos*) in a *real* laser device. The experimental results are analyzed on the basis of a discrete model derived from the Maxwell-Bloch laser equations. The model explains the parameter-independent frequency locking, the power-law dependence of the averaged energy fluctuations on the averaging region, the local decorrelation, and the chaos found in the experiments. Other characteristics of the model equations are also reported.

PACS number(s): 42.50.Lc, 42.60.Mi, 03.20.+i, 42.65.−k

I. INTRODUCTION

The study of the behavior of complex spatially extended systems has become one of the most active fields of research in recent years. Some important examples of these systems are fluids [1] and lasers [2, 3] in physics, population dynamics and differentiation of structures in higher organisms [4] in biology, and coupling between reactive cells in chemistry [5, 6]. Generally the solution of a system of evolution equations for one or various spatially extended interacting magnitudes has to be dealt with.

If the functions involved in the description of the system are continuously dependent on both space and time, the problem may be expressed as a system of partial differential equations. If the dependence on space is discrete, then the set of equations may be expressed as a system of coupled differential equations. Finally, if the time variable is discrete, we can express the problem by means of coupled maps [7]. In the simpler case when the function has only a finite set of possible values, the system is called a cellular automaton [7]. The level at which a particular problem must be considered depends on its physical nature and the information we are interested in. A complexity reduction by appropriate simplifications while retaining essential aspects of the dynamics is sometimes possible.

In laser physics, the basic equations for a two-level medium in interaction with a quasiresonant radiation field are a complicated set of nonlinear partial differential equations (PDE) for the electric field F, the matter polarization P, and the population inversion D. The latter are known as Maxwell-Bloch equations (MBE) [8] and will be explicitly described later. The level of complexity of these equations is of the same order of magnitude as the Navier-Stokes equations for fluid dynamics. Some connections between both systems of PDE's have been recently discovered [9]. For a realistic treatment the very complicated boundary conditions (i.e., the partially reflecting mirrors in the longitudinal direction or the transverse boundary conditions [10], which are usually idealized) must also be specified. The direct analysis of the time evolution of the three-dimensional space-dependent functions governing the dynamics of the laser system is far from being an easily tractable problem, even with the most powerful computers available today. Due to this high degree of complexity, many approximations are usually made, retaining some important aspects of the dynamics but eliminating others. The simpler, plane-wave approach [11, 12] is that in which only the temporal evolution of the global laser output is considered and the transverse profile is assumed to be homogeneous. The main conclusion of these studies has historically been to indicate the possibility of chaotic motion similar to that occurring in the Lorenz model of turbulence for a fluid flow [13]. Due to their simplicity, plane-wave models have been widely used to explain certain behaviors found in experimental systems, mainly to analyze the global laser dynamics [14, 15], though some conjectures have been made concerning their possible relevance in the description of local phenomena [16].

However, laser devices show not only rich temporal behaviors, but also many complex spatial features which may not be properly addressed in the framework of plane-wave or similar theories. A more refined treatment is needed for the problems of spatial symmetry breaking [17, 18], pattern formation [19], and spatiotemporal chaos [20–22]. The most common approach to these problems uses a series expansion of field, polarization, and population inversion on the basis of empty-cavity modes adapted to the considered geometry, thus reducing the 3+1 PDE system to a set of coupled ordinary differential equations for the mode amplitudes [23]. When applica-

 ©1994 The American Physical Society

ble, this approach is widely used and leads to very good results; mainly in traveling wave lasers with a low Fresnel number in the near-threshold regime [19, 24]. It is important to point out that these conditions ensure that the number of excited modes is small. In this framework, the transverse correlation lengths are of the order of the transverse section of the laser system under study [25].

Recently much attention has been paid to the so-called "defect mediated turbulence" which was theoretically predicted [26] and experimentally found in photorefractive oscillators by Arecchi and co-workers [27]. In numerical simulations of the laser equations it seems to be also present [28] and seems to be the mechanism through which the laser goes into a disordered state from the threshold in some cases (it must be noted that there are no experimental results supporting this affirmation in the laser case). Here an increasing number of topological defects appear in the system when a control parameter is varied (usually the Fresnel number) first leading to chaos and finally to turbulence when the number of defects is great enough. The lack of experimental results limits the interest of these studies.

At this point of the exposition it is interesting to point out that there are no results proving the existence of laser turbulence. In fact, most studies of transverse laser instabilities have concentrated on multimode behavior [29] and those analyzing more complex behavior have been restricted either to the near-threshold region or to purely theoretical studies. The purpose of this paper is to study phenomena in which the transverse correlation is very low, leading to strongly local phenomena which can be properly called turbulence and may not be properly described by any globally oriented model such as modal expansions. Also a theoretical model based in the assumption of weak turbulentlike behavior is analyzed in detail, together with its comparison to the experiment.

Many experimental observations in this field [21, 30, 31] remain unexplained. For the sake of completion we will briefly summarize here the main features of these phenomena. Their essential characteristic is that when measuring the intensity output in small regions of the laser spot, a chaotic oscillation is found. But when the areas measured become larger the chaotic oscillation reduces its amplitude until the output is smooth, following very simple laws such as those obtained from rate equations for lasers. So, unless the measurements are done registering small areas of the spot (e.g., using small diaphragms before the photodetectors) the existence and richness of these phenomena may be ignored. These facts indicate the existence of a local chaotic dynamic with a low transverse correlation. Another interesting feature of the dynamics is that, even though the local intensity output is chaotic, there is a (fast) predominant frequency which does not depend on the geometrical characteristics of the resonator, nor on the pumping or the losses, so that it seems to be fixed by the dynamics. In the dye laser of Ref. [30] its value is around 50 MHz. The existence of a predominant frequency has been also found in the CO_2 laser in Ref. [32] and others as will be discussed later.

Our plan is as follows. Section II presents some experimental results and a reanalysis of other previous ones. Section III presents a qualitative theoretical model and some important mathematical properties. In Sec. IV an analysis of the dynamical characteristics of our model equations and its comparison with the experimental results is made. We also discuss local chaos, transverse correlations, frequency locking, spatially averaged energy fluctuations, statistics of fluctuations, and global behavior. Finally Sec. V summarizes the overall conclusions.

II. EXPERIMENTAL FEATURES OF THE DYNAMICS OF A HIGH-FRESNEL-NUMBER, HIGH-GAIN LASER

A. Local spatiotemporal dynamics of a high-Fresnel-number dye laser

To introduce the present experimental results and to ease the comparison with the theoretical model to be presented later we analyze here the main features of the dynamics of a high-Fresnel-number, high-gain dye laser. Some of these results were reported in [30] and are included here for the sake of completeness.

The dynamics of the dye laser under study shows a very striking peculiarity. In an indirect near-field transverse correlation experiment the intensity fluctuations observed through different diameter pinholes were analyzed.

When the pinhole selected a sufficiently large area (> 0.2 mm^2) of the laser beam cross section, no fluctuations were observed, and a smooth temporal profile was registered. A reduction in the selected laser beam area permitted irregular fluctuations modulating the temporal intensity profile to be registered. When the observation area was reduced, the fluctuation amplitude rose steadily up to the 40 μm diameter pinhole, which was the smallest aperture used. Figure 1 shows the dependence of the relative energy fluctuations on the diameter (ϕ) of the external diaphragm. A power law ϕ^{α} with an exponent $\alpha = 0.84$ is found to adjust the results well. As $A \sim \phi^2$ the scaling law for the fluctuations as a function of the area of the diaphragm is: fluctuations $\sim \phi^{-0.84} \sim A^{-0.42}$. The influence of the co-

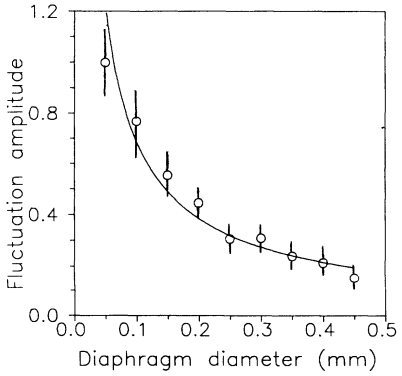

FIG. 1. Experimental dependence of the relative amplitude of the irregular fluctuations on the diaphragm diameter (which determines the region of the laser spot detected). The solid line indicates the best fit by a power function.

herence changes caused by the propagation outside the resonator was minimized by measuring only 5 cm away from the output mirror so that the power-law exponent is a real reflection of the behavior of the field inside the cavity.

An interesting result arising in the statistical analysis of the fluctuations found in a speckle pattern [33] is that the noise to signal ratio when averaging through an aperture a set of incoherent noisy speckles decays as $M^{-\frac{1}{2}}$, M being the number of speckles. Since the number of speckles is proportional to the area, the prediction for the exponent value of the power-law fitting for the area-averaged fluctuations in an incoherent or fully disordered system is $\beta = 0.5$. The anomalous exponent value found in our experiment ($\beta = \frac{\alpha}{2} \simeq 0.42$) is a reflection of the existence of some kind of order in the spatiotemporal dynamics.

An important feature of the dynamics studied in Ref. [30] is that the spectrum of the local intensity time series is relatively broadband and not reproduced from shot to shot, but when promediating many shots a very well defined frequency appears around 50 MHz. This frequency was found to be invariant when the physical parameters of the resonator were changed, and also when the pumping intensity was varied. The transmittivity of the semitransparent mirror was changed in order to modify the losses, but the value of the frequency remained invariant. No explanation was found for this phenomenon on the basis of modal analysis and other standard theories.

In order to get a deeper insight into the nature of the irregular oscillations a statistical analysis of the intensity fluctuations was carried out. We joined different pulses to get a good statistic and the result is shown in Fig. 2. As can be seen, it has a clear non-Gaussian nature. This eliminates the possibility of a purely Gaussian noise process as the origin of the fluctuations. In the case of a speckle pattern, where the intensity is the sum of uncorrelated speckles with reasonable characteristics [33], the distribution of intensity fluctuations should be a χ^2. This distribution has a clear nonsymmetrical shape and cannot be related to our experimental results, which are approximately symmetrical around the mean. This fact again supports the evidence for a not fully disordered behavior of the intensity field.

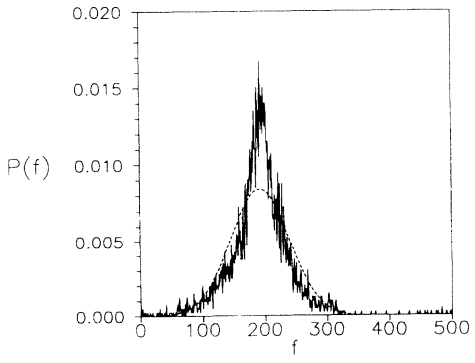

FIG. 2. Statistical analysis of the energy fluctuations. Continuous line: Probability distribution of the irregular intensity fluctuations obtained by joining different shots (4000 experimental points). The greatest fluctuation is arbitrarily assigned the value f=500 and the least one f=0. The dashed line is the fit with a Gaussian having the same mean and dispersion as that of the experimental distribution.

B. A near-field cross-correlation experiment

The averaging behavior observed could perhaps be interpreted as the superposition of many transverse orthogonal modes. This superposition would exactly cancel the local beating when the whole cross section ($S \simeq 1.8$ cm^2) is measured. Nevertheless, in the experiment the cancellation is produced when the observation area is two orders of magnitude below the whole beam cross section. On the other hand, the interpretations of the local intensity fluctuations as a local beating of transverse modes predict a high cross correlation between the fluctuations measured on different finite regions on the laser spot and the main frequency of fluctuations should be of the order of the transverse mode beating frequency. To completely clarify this point and to provide more experimental results for the comparison with the alternative explanation to be discussed later we have performed a cross-correlation experiment.

As in the early measurements [21, 30] we have worked with a coaxial flash-lamp pumped dye laser with a 15 mm near-field cross section diameter and a 500 ns pulse width. With the typical resonator lengths used the Fresnel number was around $F \simeq 100$ which greatly exceeds the theoretical prediction of Staliunas [34] for the onset of turbulence in the context of Maxwell-Bloch (and derived) models, which is $F \simeq 10$. The device is likely to provide turbulent phenomena. The high pumping achieved determines the kind of dominant instability, which should be of self-focusing type [34].

An internal rotatable Brewster window sets the polarization to 45° from the vertical plane. The output coupler is a 70% transmission dielectric mirror. A polarizing corner cube beam splitter divides the laser beam into two equally intense orthogonally polarized beams (Fig. 3). Each of the beams runs across a pinhole to fall

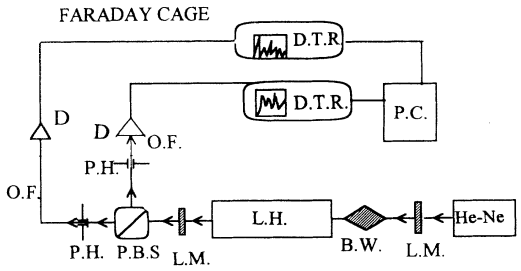

FIG. 3. Experimental setup for measuring correlations. He-Ne: He-Ne alignment laser; L.M.: laser mirror; B.W.: Brewster window; L.H.: laser head; P.B.S.: polarizing beam splitter; P.H.: pinhole; D: silicon detector; O.F.: optical fiber; D.T.R: digitizing transient recorder; P.C.: personal computer.

on the coupling window of an optical fiber cable. Both pinholes are adjustable in diameter and in their spatial location on the laser beam cross section by micrometric screws. Inside a Faraday cage the optical fiber cables are coupled to 1 ns rise time silicon photodiodes, linked to a 500 MHz real time bandwidth digital transient analyzer by a 50 Ω matched coaxial line. The laser radiofrequency strong field noise is shielded by the Faraday cage.

The two pinholes and laser mirrors are aligned by means of an auxiliary He-Ne laser. The system allows the pinholes to be placed within a circle of 0.5 mm of diameter around a point in the laser beam cross section. A more precise alignment method even allowed placement of the pinholes in a region of about 100 μm around a given point. The system is synchronized to simultaneously register the signals detected in both photodiodes. Afterwards they are subjected to a processing as described in [30] to take off the irregular fluctuations from the average behavior. Both fluctuation registers are then self- and cross-correlated in a personal computer. An extensive search was carried out over the laser spot and only *very low transverse correlations were found* (with the exception of some very near registers). This result persists even with 70 μm pinhole diameters registering areas separated by less than 100 μm (Fig. 4). These results point to the existence of a highly local decorrelation and the inexistence of appreciable global correlations, eliminating the question of mode beating as the origin of the local irregular fluctuations and leading to the interpretation presented in this paper. Thus when the detection is done over large areas the observed lack of correlation between the intensity at the different points of the pinhole area results in the cancellation of fluctuations. On the other hand, the resonator mirrors being flat, the transverse empty-cavity modes are all of the same frequency. Gain inhomogeneities could perhaps produce a breaking of this degeneracy, but the transverse mode beating could never reach the 50 MHz experimental value found for the fluctuation frequency.

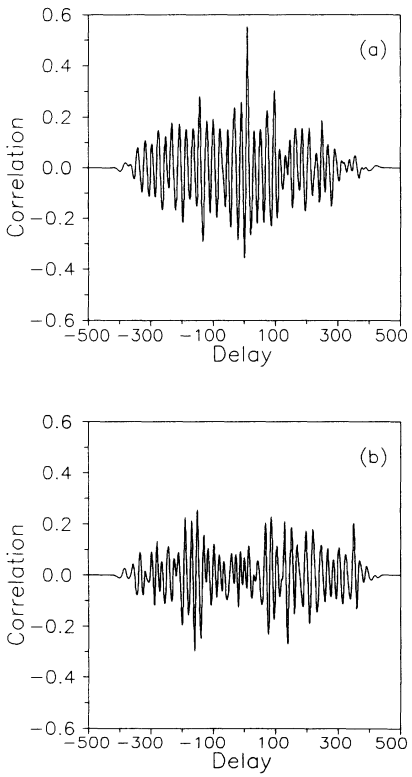

FIG. 4. Experimental cross correlations. (a) One of the better correlations found between the intensity fluctuations using 70 μm diameter diaphragms before the photodetectors. (b) Correlation when moving one of the detectors around 30 μm away from the case (a) situation. The delay is expressed in an arbitrary scale.

In conclusion, the present analysis of the experimental results of [30] together with the present experimental results allow us to make the following statements.

(1) The low correlation found in the dynamics of the dye laser supports the affirmation that *it is not of multimode type* and cannot be described by a globally-oriented model such as transverse empty-cavity mode expansions.

(2) The anomalous scaling found in the power-law fitting of the intensity fluctuations, together with the non-Gaussian nature of the statistics and the "simplicity" of the averaged spectra eliminate the possibility of a fully turbulent behavior.

All the evidence then points to the characterization of the dynamics as "weak turbulence" which is usually connected with the "existence" (perhaps in a wider sense) of local structures, their interaction giving rise to the complex behavior observed. In this dynamical regime low correlations exist but also some order remains that could explain both the anomalous scaling law and the existence of a characteristic dynamical frequency. The theoretical results to be presented in the following sections will support this affirmation.

III. THE MODEL EQUATIONS AND SOME PROPERTIES

In this section we will derive a model which will later be compared with the experiments. The starting point for our analysis is the Maxwell-Bloch equations for a polarized two-level laser in the rotating wave and slowly varying amplitude approximations [35]. Under the uniform field limit and single-longitudinal mode approximations the equations are [36]

$$-\frac{i}{4\mathcal{F}}\triangle_{\perp}F+\frac{\tilde{\epsilon}}{v}\frac{\partial F}{\partial\tau}+\tilde{\sigma}(F-P)=0\ , \tag{1}$$

$$\frac{\partial P}{\partial\tau}=-(1+i\Delta)P+FD\ , \tag{2}$$

$$\frac{\partial D}{\partial\tau}=-\gamma\left[D-r+\frac{1}{2}(F^{*}P+FP^{*})\right]\ , \tag{3}$$

where $r\simeq\frac{D_0\Lambda\alpha}{-\ln R}$, D_0 is the population inversion per atom induced by the pumping, α the small signal gain, and $R=\sqrt{R_1R_2}$ the reflectivity coefficient. Thus r is a rescaled pumping. $\Delta=\frac{\omega-\omega_0}{\gamma_{\perp}}$ is the $\gamma_{\perp}$ rescaled detuning between the fast oscillation of the field and the atomic resonance, $\tilde{\sigma}$ is a measure of the losses, including mirror

coupling this term being of the order of $\ln R$, internal transmission losses, aperture diffraction, etc., $\gamma = \frac{\gamma_\parallel}{\gamma_\perp}$ is the ratio between the depolarization time of the radiation induced material dipoles ($\gamma_\perp^{-1}$) and the lifetime of the population inversion ($\gamma_\parallel^{-1}$), $v = \frac{c}{\Lambda\gamma_\perp}$, and Λ is a characteristic length, which is usually the resonator optical length. $\mathcal{F} = \frac{\pi b^2}{\lambda\Lambda}$ is related to the Fresnel number by $\mathcal{F} = \pi F$ (b is the transverse *radius* of the mirrors). This number measures the number of Gauss-Laguerre modes which fit on the mirror apertures, so that it measures the maximum number of modes that will oscillate in the resonator. Though it is sometimes also called the Fresnel number we will call it "maximum mode number" to avoid confusion.

The domain of the transverse rescaled variables $\chi = \frac{x}{b}, \eta = \frac{y}{b}$ is $[0,1]$ (for a square geometry) no matter what size the transverse section is. Some elementary algebraic transformations [16] have been done on the standard form of the Maxwell-Bloch equations to write them in the form (1)–(3), so that they are more practical for our purposes. In principle, the factor $\tilde{\epsilon}$ is a complex number (optical dielectric permittivity) including the internal absorption which takes other physical processes in the medium into account as described in Ref. [16]. From now on this will be considered a real quantity. Finally $s = \gamma_\perp t$ is a rescaled time variable. The restriction made to the consideration of polarized fields is not important for the phenomena we want to analyze here and corresponds to the experimental setup used in the cross-correlation experiment. In a general case the consideration of arbitrary, nonfixed, polarizations may give rise to new phenomenology [37].

The theoretical approach proposed in this paper consists of the consideration of a finite bidimensional array of adjacent lasing structures or filaments coupled by the nearest neighboring diffracted field. For the sake of simplicity we take a square lattice with spatial period h as the bidimensional distribution of lasing structures. The model equations are then the following discrete version of (1)–(3):

$$\dot{F}_{ij} = \sigma(P_{ij} - F_{ij}) + ig(F_{i+1j} + F_{i-1j} + F_{ij-1} + F_{ij+1} - 4F_{ij}) , \tag{4}$$

$$\dot{P}_{ij} = -(1 + i\Delta)P_{ij} + F_{ij}D_{ij} , \tag{5}$$

$$\dot{D}_{ij} = -\gamma\left\{D_{ij} - r + \frac{1}{2}\left(F_{ij}P_{ij}^* + F_{ij}^*P_{ij}\right)\right\} , \tag{6}$$

$$i, j = 1, 2, ..., N$$

where $\sigma = \tilde{\sigma}\frac{v}{\tilde{\epsilon}}$.

From now on these equations will be referred to as discrete Maxwell-Bloch equations (DMBE). The set of laser oscillators is described by the local fields $\{F_{ij}, P_{ij}, D_{ij}\}$ and they are coupled by a term simulating the nearest neighbor diffracted field, the g coefficient being the coupling constant. We do not use the discretization as a trick to enable an easier analysis of the nondiscretized set (1)–(3) but try to give a meaning to the structures presented here as will be discussed later. The coupling coefficient may be taken proportional to $g \sim \frac{\tilde{v}}{4h^2\mathcal{F}}$, h being a distance between the laser oscillators, but many other effects can be taken into account in the coupling constant g. For example, the formation of solvatation shells around the dye molecules may act as a screening of the interaction between filamentary structures, etc. What is clear is that, as the continuous limit of the discrete coupling term is the Laplacian term, if the transverse dimension b is held constant, the value of g in that limit can be inferred to be

$$\lim_{N\to\infty} g(N) = \frac{\tilde{v}N^2}{4\mathcal{F}} \tag{7}$$

but this is true only in the continuous limit where the structures have no sense anymore. For example, when the size h of the structures is given a physical meaning (is fixed) an increase in N leads to an increase of the total transverse size b. The discrete model is thus independent of the continuous limit and g can be taken freely.

Similar approaches to complex problems have been followed in many physical problems, e.g., the analysis of Rayleigh-Bernard turbulence [38], in the original Turing analysis of spatial instabilities [5], in reaction-diffusion equation-based models [7] and in the analysis of the Ginzburg-Landau equation [39]. In these cases, the simplification is usually physically meaningful when the dynamical system has a "coarse grained" dynamics, i.e., finite size coherent structures exist with any kind of mutual interaction giving rise to complex behavior. In our case, candidates for these structures have been experimentally detected [40] and theoretically proposed on the basis of the DMBE's; these are the filamentary or condensate structures analyzed in Refs. [41, 42]. In fact, the adiabatically reduced Maxwell-Bloch equation [18], which is expected to retain many essential aspects of the dynamics of the whole set of MBE's (though probably not all [43–45]), has a term that behaves as focusing and can dynamically compensate the diffraction in order to give rise to characteristic scale structures. In an interesting work, Emelyanov and Yukalov [46] explained the formation of these filamentary structures on the basis of the global energy reduction in the filamented state as compared with that of the homogeneous state. Despite the very crude approximations made, they calculated the laser domain sizes, their dependence on the resonator length, and the influence of the Fresnel number on the filamentary domain formation. Their results are in qualitative (and sometimes even quantitative) agreement with some experimental results, as was pointed out in [16].

Aside from the origin of these structures, two facts are clear: (1) experimental evidence supports its existence (perhaps even multimode and other types of ordered patterns might be described as arrays of "filamented structures") and (2) in the regime where these structures are present, the local dynamics should almost be determined by the plane-wave equations plus an interaction with nearby structures with negligible influence of boundary conditions. This affirmation is supported by the results in Ref. [30]. Thus Eqs. (4)–(6) are a reasonable model for the dynamics of a system with such structures. It is expected that the model will work better in the weak coupling regimes.

Thermal effects will not be considered here, but an influence of the temperature has been found in some cases [30], though it is probably due to the enhancement of the noise unavoidably present in the system and to the effect on the nonradiative transitions of the dye molecules.

The g coefficient depends on the maximum mode number through $\frac{1}{F}$. Since diffraction is known to increase the coherence [47], the decrease in the Fresnel number leads to strongly coupled and probably coherent structures, thus favoring homogeneous and/or coherent spots, while the increase in the Fresnel number (due to an increase in the transverse size) leads to greater independence of the dynamics so that the formation of ordered coherent patterns will probably be unfavored. The stability analysis will support this affirmation.

It must be noted that this model is not supposed to be a good one, except when in the turbulent regime in which the assumptions made in its establishment have any sense. Of course it will not give any information on the ordered patterns arising near the threshold in moderate-Fresnel-number lasers. In those systems the boundaries play an essential role [48], which is not so here. To do an analysis of these systems multimode expansions or direct numerical simulations of the Maxwell-Bloch equations are likely to be the better approaches.

We insist that we interpret the model not just as a way to integrate numerically the Maxwell-Bloch equations (for this purpose a finite-difference approach [49] would be preferable) but as a system of coupled structures that may have sense as the theoretical and experimental evidence points out. The model here developed can be applied to analyze any system of diffractively coupled lasers, as it happens in semiconductor laser arrays [50, 51] or in coupled CO_2 cavities [52]. As our equations exactly represent a bidimensional array of coupled single-longitudinal mode lasers and this is sometimes the experimental setup, the agreement of our model with the experiment is expected to be very good in some cases. The particular value of g can be obtained from the physical mechanism providing the interaction and thus the comparison between theory and experiment should be simple. More details on this application of the model will be given later. Preliminary theoretical studies in this direction were done by Otsuka [53] in the context of linear arrays of coupled waveguide lasers.

At this point we will proceed from the DMBE's and justify their validity by the physical relevance of the results. The system is furthermore interesting from a mathematical viewpoint, because of some curious dynamical features of the DMBE's to be discussed later.

From now on the set of fields $\{F_{ij}, P_{ij}, D_{ij}\}$ will be called "oscillator" or "filament." In the statement of the coupling term in (4) we have chosen a square lattice. Other more complicated symmetries (or even a random distribution) are also possible, but probably equivalent, provided we are restricted to only qualitative results. The independence of g with both the point and direction in the lattice guarantees the homogeneity and isotropy properties, which are to be expected.

From now on, and for the sake of simplicity, we will assume transverse periodic boundary conditions. However, no qualitative differences were found in the *dynamical behavior* of the DMBE's in the disordered region using zero boundary conditions and Gaussian pumping (these results will be presented in Sec. IV).

Some important properties of the model will now be presented. The change in variables

$$x_{ij} = \sqrt{\gamma} F_{ij},\ y_{ij} = \sqrt{\gamma} P_{ij}, \text{ and } z_{ij} = r - D_{ij}$$

is useful so that the model equations are in an equivalent form to the standard form of the complex Lorenz equations (CLE) [12] with the difference of the coupling term.

$$\dot{x}_{ij} = \sigma(y_{ij} - x_{ij}) + ig(x_{i+1j} + x_{i-1j} + x_{ij-1} + x_{ij+1} - 4x_{ij}), \tag{8}$$

$$\dot{y}_{ij} = -(1 + i\Delta)y_{ij} + x_{ij}(r - z_{ij}) , \tag{9}$$

$$\dot{z}_{ij} = -\gamma z_{ij} + \frac{1}{2}(x_{ij} y^*_{ij} + x^*_{ij} y_{ij}) . \tag{10}$$

There evidently exist infinite homogeneous solutions of the form

$$x_{ij} = X,\ \ y_{ij} = Y,\ \ z_{ij} = Z,\ \ \forall i, j = 1, ..., N ,$$

(X, Y, Z) being any solution of the CLE's.

Before going on in the analysis of the DMBE's we will summarize some dynamical features of the complex Lorenz equations [12]. The main result is the existence of an exact periodic (limit cycle) solution for field and polarization while the population inversion remains at a constant value

$$X = Ae^{i\omega\tau},\ \ Y = A\left(1 + i\frac{\omega}{\sigma}\right)e^{i\omega\tau},\ \ Z = \frac{|A|^2}{\gamma} , \tag{11}$$

where $|A| = \sqrt{\gamma(r - r_1)}$, $r_1 = 1 + \frac{\Delta^2}{(\sigma+1)^2}$, $\omega = -\frac{\sigma\Delta}{\sigma+1}$. Under an increase in the pumping over a critical value r_1 (representing the laser threshold), the stationary (nonlasing) solution $X = Y = 0$ becomes unstable and the limit cycle becomes the stable (lasing) solution. Only if both $\sigma > \gamma + 1$ and $r > r_2$, r_2 being the well-known "second threshold," does the limit cycle solution become unstable, in which case chaos may appear. An important characteristic of the DMBE's is that their solutions are bounded, as is proven in Appendix A.

Following the notation of [55] and using the results in Appendix A, it is clear now that the DMBE system has an absorbing set. The proof is very simple because any ball $B(0, \rho)$ with a radius $\rho > \rho_0$ centered at the origin is already an absorbing set. Let $\mathcal{B}_0$ be a bounded set in H and $B(0, R)$ a ball with a radius $R > \rho_0$ containing it, then $S(\tau)\mathcal{B}_0 \subset B(0, \rho)$ for $\tau \geq \tau(\mathcal{B}_0)$ being

$$\tau(\mathcal{B}_0) = \frac{1}{2l} \ln \frac{R^2 - \rho_0^2}{\rho^2 - \rho_0^2}$$

and $S(\tau)$ the action of the flow on the ball.

Additionally the balls with a radius greater than ρ_0 are positively invariant, in the sense that $S(\tau)B(0, \rho) \subset B(0, \rho), \forall \tau \geq \tau_0$. It may be proven that the dynamical

system has a bounded maximal attractor in the sense of [55].

Another interesting property is that the CLE's are invariant under the change

$$F \to Fe^{i\varphi} \; P \to Pe^{i\varphi} \; D \to D \; . \tag{12}$$

The existence of a zero eigenvalue in the coefficient matrix of the linearized system is essentially linked to this property of symmetry, which may be explicitly used to reduce the order of the dynamical system. Let us define the new variables $x = ae^{i\varphi}$, $y = be^{i\psi}$, $z = c$. After some straightforward algebra, it is found that

$$\begin{aligned} \dot{a} &= \sigma b \cos(\beta) - \sigma a \; , \\ \dot{b} &= -b + ac\cos(\beta) \; , \\ \dot{\beta} &= -\Delta - \sin(\beta)\left((r-c)\frac{a}{b} + \sigma\frac{b}{a}\right) \; , \\ \dot{c} &= \gamma\left[-c + ab\cos(\beta)\right] \; , \end{aligned} \tag{13}$$

where $\beta = \psi - \varphi$. The dynamical system has been formally reduced from fifth to fourth order. Thus, in the special case $g = 0$, the DMBE may be reduced from $5N^2$ to $4N^2$ order. This is due to the local invariance under the phase change

$$F_{ij} \to F_{ij}e^{i\varphi_{ij}} \; P_{ij} \to P_{ij}e^{i\varphi_{ij}} \; D_{ij} \to D_{ij} \tag{14}$$

due to the decoupling. When the coupling is introduced the local phase invariance is broken and only the global phase changes $F_{ij} \to F_{ij}e^{i\varphi} \; P_{ij} \to P_{ij}e^{i\varphi} \; D_{ij} \to D_{ij}$ remain as a valid symmetry. The coupling instantaneously increases the total effective number of degrees of freedom by $N^2 - 1$ due to the lost symmetries.

Once the pumping reaches a critical value the lasing state is established. What that lasing state is and what its parameter region of stability is will be discussed in Appendix B because it is not essential for the results presented here. The reason is that the first lasing state appears in the low pumping and low-Fresnel-number region in which the model is of no physical applicability.

IV. COMPARISON OF THE DYNAMICAL DMBE BEHAVIOR WITH THE EXPERIMENTAL RESULTS

A. Numerical simulation details

Now to be reported and discussed are the results of the numerical integrations of the DMBE's. The integrations were carried out on a VAX9000, a DEC-ALPHA, a Convex C-210, and various i486-type computers using a fourth-order Runge-Kutta method. The accuracy of the solutions was checked using different time steps.

The variables from which the dynamical information is extracted are the local fields $\{F_{kl}, P_{kl}, D_{kl}\}$, the local energy (or intensity) $I_{kl} = \mid F_{kl} \mid^2$, and the global intensities $I_N = \sum_{k,l} I_{kl}, k, l \in N$, N being any subset of the full set of oscillators. These global intensities are the ones we measure in experiments using wide-area detectors.

Although wide regions of the parameter space were integrated, our attention will focus on the more physical regions. The parameters for the usual lasers are in the region $\sigma \simeq 0.1 - 0.3$, $\Delta \simeq 0.1 - 0.5$. The pumping r may achieve very high values in the pulsed lasers of Refs. [30, 31] from the threshold $r \simeq 1$ up to $r \simeq 80$. The γ parameter varies from $\gamma \simeq 0.1 - 1.0$ for the dye laser of Ref. [30] to $\gamma \simeq 0.001$ for the pulsed CO_2 case of Ref. [31].

B. Overview of the local chaotic dynamics and correlations

The DMBE's present a very rich dynamical behavior in the different parameter regions. In typical cases a local chaotic dynamics exists [Figs. 5(a) and 5(b)], but pattern formation and other coherent behaviors have been found for concrete parameter values. Even in these cases a long irregularly oscillating transient is found before an ordered pattern arises. The regions in which the simulations were more exhaustive are described in Sec. IV A. We performed some numerical simulations to see the effect of the different types of instabilities on the behavior of the system. The first exploration was for case I (pulsed CO_2 lasers) with $\sigma = 0.1, \Delta = 0.3, r = 40, g = 0.1, \gamma = 0.001$. For a number of domains ($N = 6$) below the critical value for type I instability (see Appendix B for details) all the modes lie in the type II instability region [see Fig. 16(a) in Appendix B] and the behavior is chaotic with a fast predominant frequency as will be discussed in Sec. IV D. When we increase the number of domains ($N = 9$), some

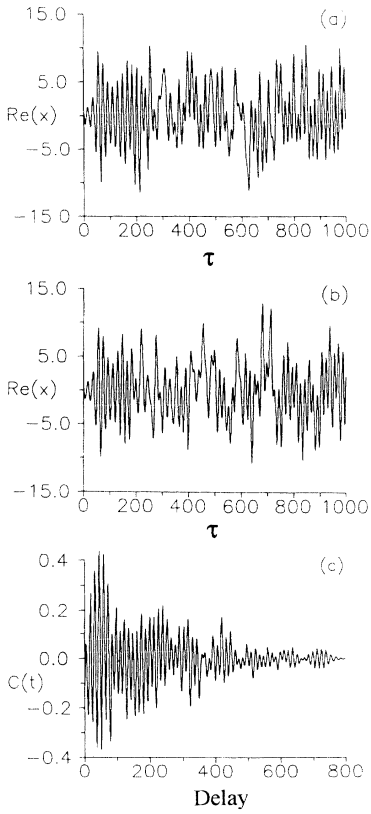

FIG. 5. (a) and (b) Local chaotic dynamics for neighbor oscillators and (c) the field correlation functions for a random-initial-conditions (RIC) case (see text) and parameter values $\sigma = 0.1, \Delta = 0.3, g = 0.1, \gamma = 0.001, r = 40.0$.

modes fall into the type I instability region and the frequency decreases. A further increase in N ($N = 20, 30$) enhances this tendency. In this case these results point to the existence of different attractors, which are reached by the different instabilities. Instability type I seems to favor a low frequency behavior while the instability type II seems to favor a high frequency instability. This is not so for case II parameters, where only type I instability is present and leads to a fast frequency attractor, which is the only one seen in this parameter range.

No matter how the instability develops (which may be model dependent) the important point is that in the chaotic states (both in the transient irregularly oscillating states and in the stationary chaotic states) the cross-correlation function between nearby oscillators decays very quickly [see Fig. 5(c)]. In fact, in many cases no appreciable correlations between the time series of the field of nearby oscillators were found [see Fig. 5(c)]. The correlation function between the intensities of nearby local oscillators (Fig. 6) is analogous to the experimental results of the correlation function in Sec. II, thus showing a great similarity with the experimental results reported.

The structure of the local attractor is very complicated, as Fig. 7 shows. The boundary conditions were found to have little or no importance for the dynamical behavior in the disordered stages as it should be, provided the physical meaning of the model. To be specific we integrated some cases with periodic and zero boundary conditions without essential changes. We also studied the effect of a nonphysical boundary condition which was a variant of the periodic ones. The only difference was that the real part of the field in one side of the lattice was connected, not with the field on the other side, but with the real part of the polarization. This change seemed not to affect the results.

In general, the energy is very well distributed between the oscillators so that the entropy defined as

$$S(\tau) = -\frac{1}{2\ln N}\sum_{k,l=1}^{N}\frac{I_{kl}}{I(\tau)}\ln\left(\frac{I_{kl}(\tau)}{I(\tau)}\right) \tag{15}$$

is almost constant and very near the equipartition value $S = 1$ (Fig. 8). When using spatially nonuniform pumping, the energy is (on average) distributed across the lattice following the pattern imposed by the pumping.

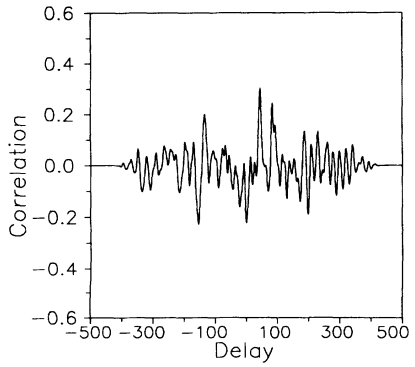

FIG. 6. Correlation function between the intensity fluctuations of two nearby oscillators for dye laser parameters. The delay is expressed in an arbitrary scale. Parameter values of the simulations $\sigma = 0.3, \gamma = 0.5, \Delta = 0.3, g = 0.1, r = 40$.

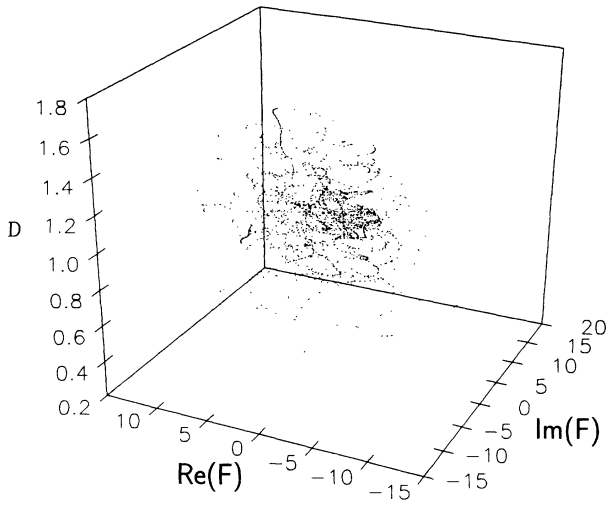

FIG. 7. Projection of the local attractor on the (F, P, D) space. Parameter values are $\sigma = 0.1, \Delta = 0.3, r = 40, \gamma = 0.001, g = 0.1$.

C. Spatially averaged fluctuations

The decorrelation of the local dynamics is also manifested by the behavior of the energy fluctuations when they are averaged over different areas [56] as was pointed out in the experimental section.

To compare the model results with the experimental ones we have calculated the time average of the integrated intensity fluctuations

$$\Delta_{mn}I(r) = \left\langle \frac{\sum_{k,l\in B_{mn}(r)} I_{kl}(\tau) - \left\langle \sum_{k,l\in B_{mn}(r)} I_{kl}(\tau') \right\rangle}{\bar{N}_B(r)} \right\rangle \tag{16}$$

for numerical time series obtained from the DMBE's. The brackets $\langle\rangle$ denote a time average: $\langle\rangle$ =

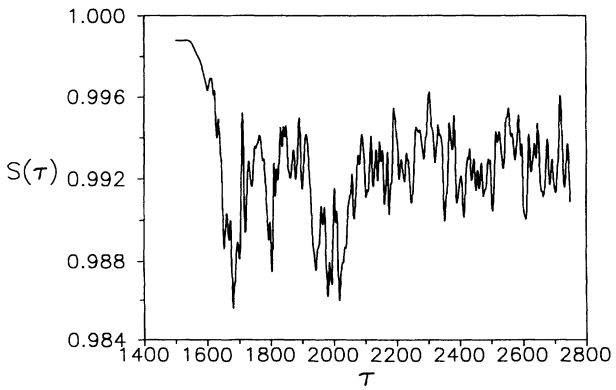

FIG. 8. Time evolution of the entropy for a particular case. Parameter values $\sigma = 0.3, \Delta = 0.3, r = 40, \gamma = 0.5, g = 0.1$

$\frac{1}{\tau_f-\tau_i}\int_{\tau_i}^{\tau_f} d\tau$. $B_{mn}(a)$ is the ball with a radius a centered on an arbitrary oscillator mn. The particular election of mn was found to be unessential because of the mean independence of the dynamics on the concrete point on the lattice and the long time average. $\bar{N}_B(a)$ is the number of oscillators in the ball $B_{mn}(a)$. The distance is taken in the sense of "interaction" so that $d(kl,ij) = |k-i|+|l-j|$ (this is the natural metric for the lattice).

A very interesting result is shown in Fig. 9. The decay of the spatially averaged fluctuations for parameter values in the dye region is well adjusted by a power law, $\delta E(A) \sim A^{\beta}$, A being the area registered (measured by the number of oscillators) with an exponent $\beta \simeq 0.41$ for parameter values $\sigma = 0.2, r = 80, \Delta = 0.3, g = 0.1, \gamma = 0.1$. The value of this exponent is not a consequence of a fortunate election of the parameters. For example, for parameter values $\gamma = 0.2, \sigma = 0.2, \Delta = 0.3, r = 40$ and $\gamma = 0.5$, $\sigma = 0.1$, $\Delta = 0.3, r = 40$ the exponents found when averaging the energy fluctuations for three shots were $\beta = 0.40 \pm 0.02$ and $\beta = 0.40 \pm 0.01$, respectively.

This dependence is characteristic [56] of the so-called weak turbulence or spatiotemporal chaos, which corresponds to the evolution of coherent structures having the size of the correlation length. This is a more ordered state than the fully developed turbulence, which implies an exponent $\beta \simeq 0.5$.

This result is in good quantitative agreement with the previously described experimental results and provides additional evidence for the existence of something like coherent structures in the real behavior of the dye laser.

D. Dynamical frequency locking

Another important characteristic of the dynamics is that the averaged Fourier spectrum of the time series of the local intensities shows a peak in a frequency value (and sometimes in its harmonics) which is almost invariant under parameter changes in the physical region. Figures 10(a)–10(d) show the independence of this frequency under some parameter variations. The figures were obtained computing the maximum of the average power spectrum of different shots (typically three or four) for each value of the parameters. Our search region included $\gamma \in [0.001, 1.0], r \in [10, 100], \sigma \in [0.01, 2.0], g \in [0.0, 1.0]$. This frequency has nothing to do with modal separations etc., and is the result of a curious dynamical frequency locking. This locking appears both in the parameter regions where the system is ordered and in the chaotic regimes (though here the spectrum is more complex). This frequency grows linearly with the coupling constant g for small values of this parameter in a way to be discussed later. For larger g values, the monotonously increasing behavior ends and an independence of the dynamical frequency value on the coupling parameter is found [Fig. 10(e)].

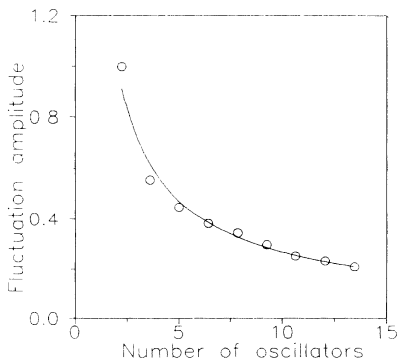

FIG. 9. Numerical simulations of the dependence of the amplitude of the intensity fluctuations on the averaging region; parameter values are $\sigma = 0.2, r = 80, \Delta = 0.3, g = 0.1, \gamma = 0.1$. The solid line indicates the best fit by a power function.

It is remarkable that the locking frequency cannot be related to any of the other system parameters in the parameter region studied. A semiphenomenological explanation will be given in Sec. IV E, but it is far from being complete. The phase-locking and frequency-locking behavior of collectivities of coupled nonlinear oscillators seems to be well established [57], but the locking frequency is usually a characteristic (natural) frequency of the oscillators or some kind of mean when they have the same natural frequencies. The interest of the coupling found here lies in the fact that the common frequency is independent, not only of the natural frequencies of the oscillators but also of the parameter values in a wide region of the parameter space.

As the time variable in our model equations is scaled by $\gamma_\perp$, the physical value of the frequency (ν_{expt}) is obtained from the numerical one (ν_{num}) by the transformation

$$\nu_{\text{expt}} = \nu_{\text{num}}\gamma_\perp . \tag{17}$$

Considering that for the dye laser $\gamma_\perp \sim 10^9$ s^{-1}, it is found that the value of the frequency, in physical units, is around 10^2 MHz. This is then of the same order of the frequency found in the experimental local intensity time series as discussed in Sec. II. This fact provides more evidence that the discrete model retains some essential features of the dynamics.

The CO_2 laser of Ref. [32] also presents the existence of a dynamical frequency which has no clear origin having a value of around 500 kHz. Because the values of the relaxation constants are different from those for the dye, the difference between the numerical values might be explained. Perhaps that system is also showing another case of this kind of frequency locking. More experimental information should be necessary to make a concrete comparison.

In semiconductor coupled laser arrays chaotic dynamics is also found, as is discussed, for example, in Ref. [50]. There the number of elements seemed not to be large enough to get a complete frequency locking, at least it is not clear in the global intensity shown in Figs. 1–5 in [50], but local measurements for each laser field may clarify it. However, the order of magnitude of the dynamical frequency arising there is one or two orders of magnitude larger than the one found in our laser, which again approximately matches with the differences in the $\gamma_\perp$ value

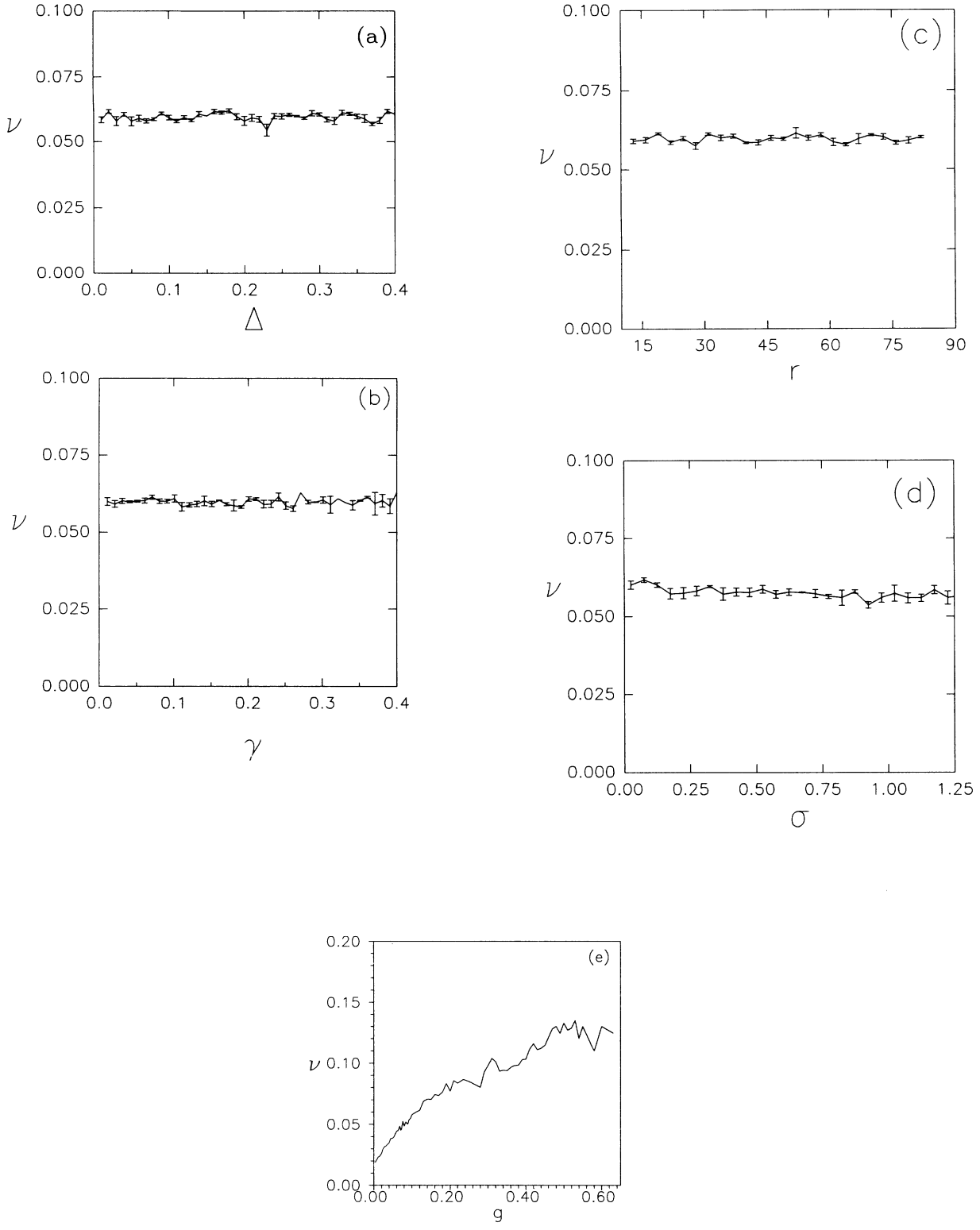

FIG. 10. Dependence of the "fundamental" dynamical frequency on the system parameters (a) $r = 40, \gamma = 0.5, g = 0.1, \sigma = 0.3, \Delta \in [0.01, 0.4]$, (b) $r = 40, \gamma \in [0.01, 0.4], g = 0.1, \Delta = 0.3, \sigma = 0.3$, (c) $\gamma = 0.5, g = 0.1, \Delta = 0.3, \sigma = 0.3, r \in [10, 90]$, (d) $r = 40, g = 0.1, \sigma = 0.3, \Delta = 0.3, \sigma \in [0.05, 1.25]$, (e) $r = 40, \gamma = 0.5, \Delta = 0.3, \sigma = 0.3, g \in [0.004, 0.63]$.

and may be the larger g value because of stronger coupling that is likely to be there.

E. Dynamics in the dye laser parameter region

We will concentrate now on the dynamics in the dye laser parameter region in which some special features appear, allowing a more complete explanation of some of the observed phenomena.

When near-homogeneous initial conditions are used, a long transient is found before the complex behavior appears; this is due to the fact that only type I instability with very small positive indexes is present and a few modes lie inside the instability region so that it needs time to develop.

The numerical simulations show the striking fact that the local dynamics takes place (very approximately but not exactly) on the codimension 2 hypersurface defined by the equations

$$\frac{|F_{kl}|^2}{r-r_1} = \frac{r_1}{D_{kl}} , \tag{18}$$

$$\frac{|P_{kl}|^2}{r-r_1} = D_{kl} . \tag{19}$$

A typical case is shown in Fig. 11. In the unperturbed case ($g = 0$) the dynamics takes place on a line inside these surfaces (the limit cycle). In the coupled case ($g \neq 0$) the dynamics becomes very complex but the trajectory lies very approximately inside this set which we think is not trivial. Let us remember that when γ is small the dynamics is far different in the sense that the trajectory does not lie on a simple surface.

Figure 12 shows some typical features of the dynamics in this parameter region. The amplitudes $a_{kl} = |F_{kl}|$ and $b_{kl} = |P_{kl}|$ perform oscillations around the value corresponding to the unstable limit cycle $a_{kl} = \sqrt{r-r_1}$, while the phase φ_{kl} has a very fast evolution with the characteristic frequency discussed above so that $a_{kl}\dot{\varphi}_{kl} \gg \dot{a}_{kl}$. The polarization follows the same behavior and is moreover slaved by the field, allowing even the crudest adiabatic elimination (zero order) to be applied with a very high degree of approximation.

Taking into account these facts, and concentrating in the small g and $\Delta > 0$ region, where the fluctuations around the stationary values are small, a deeper understanding of the frequency locking can be given. The model equations in the approximation discussed before are

$$\begin{aligned} ia_{kl}\dot{\varphi}_{kl} = &-\sigma a_{kl} + \frac{\sigma a_{kl} D_{kl}}{1+\Delta^2}[1 - i\Delta] \\ &+ ig(a_{k+1l}e^{i\varphi_{k+1l}} \\ &+ a_{k-1l}e^{i\varphi_{k-1l}} + a_{kl+1}e^{i\varphi_{kl+1}} \\ &+ a_{kl-1}e^{i\varphi_{kl-1}} - 4a_{kl}e^{i\varphi_{kl}})e^{-i\varphi_{kl}} , \end{aligned} \tag{20}$$

$$\dot{D}_{kl} = -\gamma\left(D_{kl} - r + \frac{a_{kl}^2 D_{kl}}{1+\Delta^2}\right) . \tag{21}$$

The numerical simulations show that when g is very small, the population inversion remains near the thresh-

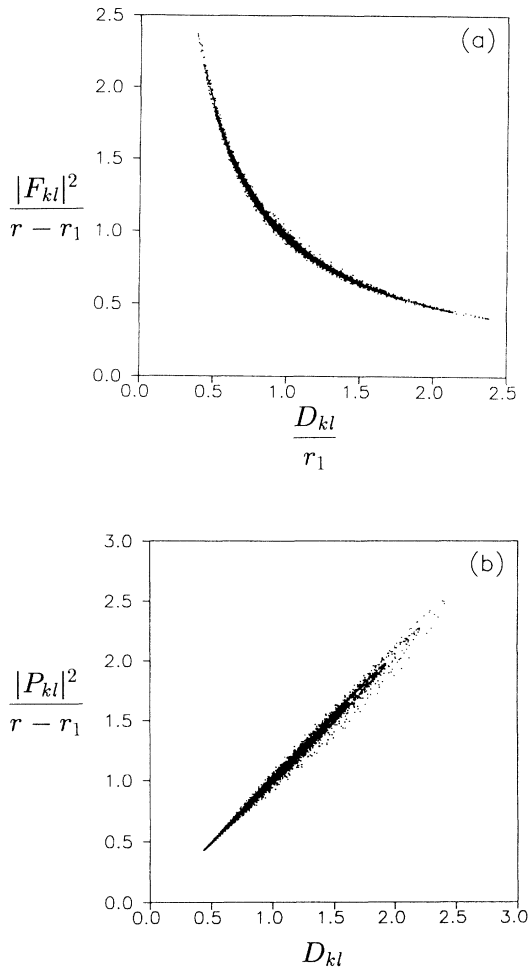

FIG. 11. (a) Phase portrait showing $|F_{kl}|^2/(r-r_1)$ vs D/r_1. As can be seen, the points lie spreading a bit around the curve $y = 1/x$. (b) Phase portrait showing $|P_{kl}|^2/(r-r_1)$ vs D_{kl}. The points lie near the curve $y = x$.

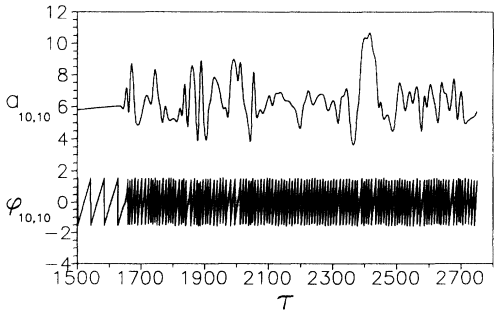

FIG. 12. Local time series of the intensity and phase for an oscillator in the lattice. The phase φ is shown in the lower part and is a rapidly changing function (we have artificially restricted it to the interval $[0,2\pi]$) while the amplitude is shown in the upper part. Parameter values are $\sigma = 0.3, \Delta = 0.3, r = 40, \gamma = 0.5, g = 0.1$.

old ($D_{kl} \simeq 1 + \Delta^2$) and the amplitude fluctuations are very small. Also, in our rough approximation we will substitute $1 + \Delta^2 \simeq 1$. Taking this fact into account, the equations reduce to a simpler form. Defining new phase and time variables by

$$\psi_{kl} = \varphi_{kl} - 2\pi\nu_0\tau \ , \tag{22}$$

$$u = g\tau \ , \tag{23}$$

where $\nu_0 = \frac{\sigma\Delta+4g}{2\pi}$, the form of the equation is found to be

$$\frac{d\psi_{kl}}{du} \simeq \cos(\psi_{k+1l} - \psi_{kl}) + \cos(\psi_{k-1l} - \psi_{kl}) + \cos(\psi_{kl+1} - \psi_{kl}) + \cos(\psi_{kl-1} - \psi_{kl}) \ . \tag{24}$$

Numerical simulations of phase equation (24) are shown in Fig. 13. It is clear that ψ evolves slowly as compared to φ, which includes a monotonously increasing component. The analytical prediction matches with the numerical results on the very low g limit. For example, for a particular case, and using the ν values found for $g = 0.004$ and $g = 0.008$, the adjustment was $\nu_0 = 0.014 + 0.58g$, which is very near the predicted $\nu_0 = 0.018 + 0.64g$.

In the parameter region in which the approximations are valid, $\sigma \simeq 0.1, \Delta \simeq 0.1, g \simeq 0.1$, the g component of ω_0 dominates when g is not too small. Taking into account that the physical values of σ and Δ are small, the locking frequency is likely to be almost independent of them. This result points to the fact that the locking of the laser oscillators has to do with the phase of the fields and the phenomena analyzed here (despite the complexity of the system) have their origin in the phase locking.

However, the saturation behavior for larger g values cannot be so simply explained out of the region of validity of the approximations made here.

F. Statistics of the intensity fluctuations

In the dye laser parameter region the statistics of the intensity fluctuations around the mean were analyzed to compare with the experimental results discussed in Sec. II A. Two numerically simulated time series of the intensity for parameter values in the dye region were subjected to the same processing as the experimental registers and a similar number of points was taken to build a statistic of energy fluctuations. The results are shown in Fig. 14 and again a very good match between theory and experiment is found. The best agreement concerns the shape (non-Gaussian) of the distribution and the position of the maximum of the distribution. The comments made in Sec. II A concerning the comparison with the speckle distribution are applicable here.

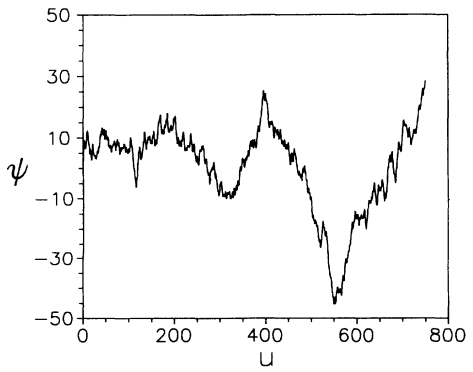

FIG. 13. Numerical simulations of the phase evolution obtained with the reduced phase equation showing that ψ_{kl} evolves slowly as compared to φ.

G. Global relaxation oscillations

Another interesting feature of the simulations is that for many parameter values the global intensity (corresponding to the detection of the full laser spot) shows an oscillating relaxation behavior towards a stationary state as is observed under certain experimental conditions.

The global intensity $I(t)$ for $r = 10, \gamma = 0.001, \sigma = 0.1, \Delta = 0.3, g = 0.1$ is shown in Fig. 15 for two different kinds of initial conditions. The first ones were a constant value plus a small amplitude Gaussian centered on the middle of the lattice [Gaussian initial condition (GIC)] and are shown in Fig. 15(a). The second ones were a constant value plus a small amplitude white noise [Fig. 15 (b)]. It is not surprising that in the case of a more uncorrelated (random) initial condition (RIC), the decay to the stationary state is faster than in the correlated one.

It should be pointed out that the frequency of these "relaxation oscillations" in case I coincides with the frequency of the relaxation oscillations in class B lasers (because the parameter values are in that range) $\omega = \sqrt{2\sigma\gamma(r-1)}$. It is interesting how our discrete theory reproduces this behavior, even when the local dynamics is so complicated.

On the other hand, as the intensity of each element on the lattice oscillates around its equilibrium value (now unstable) the total intensity is just N^2 times the equi-

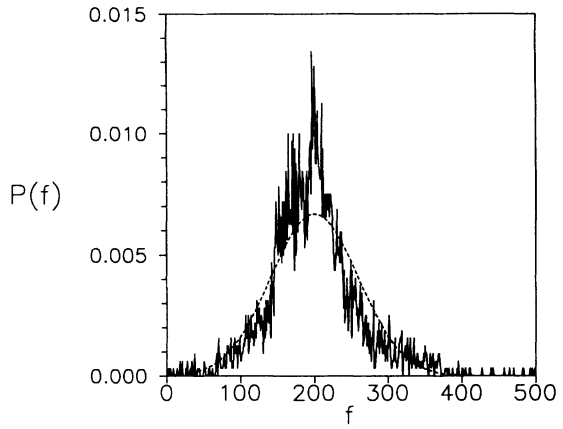

FIG. 14. Statistical analysis of the energy fluctuations. Continuous line: Probability distribution of the irregular intensity fluctuations obtained using 3500 points for two different cases. The greatest fluctuation is arbitrarily assigned the value f=500 and the least one f=0. The dashed line is the fit with a Gaussian having the same mean and dispersion as that of the numerically obtained distribution. Parameter values for the simulations were $\gamma = 0.5, \Delta = 0.3, r = 40, g = 0.1, \sigma = 0.3$.

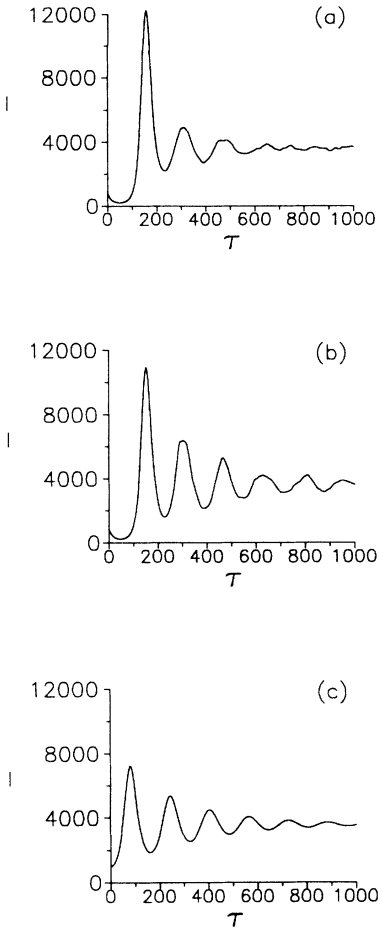

FIG. 15. Global dynamics for parameter values $\sigma = 0.1, \Delta = 0.3, r = 10, \gamma = 0.001, g = 0.1$. (a) corresponds to random initial conditions, (b) corresponds to smooth (Gaussian) initial conditions, and (c) is the result of an integration with $g = 0.0$ which is included for comparison.

librium value for each oscillator once the transient has died [$I_{\text{tot}} \to N^2 \times (r - r_1)$]. At first sight, there seems to be only a slight change in the global dynamics when the coupling is introduced. In fact, the comparison of the curves in Figs. 15(a) and 15(b) with the time evolution obtained with $g = 0.0$ and GIC conditions [Fig. 15(c)] shows only slight differences, the main one being that the coupled system output is slightly noisy [see, for example, the tails of $I(t)$ in Fig. 15] because of small noncompensations of the deviations from the mean values of local intensity oscillations, which is not so for the uncoupled system. There, each oscillator performs a relaxation oscillation so that all the oscillators contribute exactly with the same intensity value to the total intensity. The pumping effect on global dynamics is a reduction in the decay time of the oscillations so that using $r \geq 40$ and GIC, only one or two oscillations can be distinguished.

Due to the similarity between the coupled and uncoupled global dynamics, a few changes should be expected in the local behavior. However, this is not the case, as we have seen in the previous sections. In fact, the promediation of the complex local dynamics to seemingly smooth outputs has permitted these experimental phenomena to be hidden for many years and it is probable that they are present in many laser systems.

These results are somewhat striking, because despite the decorrelation of the dynamics at a local level, a highly regular oscillation arises in the global profile of the intensity. This may be concisely expressed as *"disorder + disorder = order."* It is also important to note that this order is not a consequence of random statistical behavior, because there are clear deterministic oscillations in the global intensity profile for much longer times than the local field correlation times, indicating that there is some kind of global organization. From the viewpoint of stability it may be hypothesized that the oscillation of the unstable linear modes promediates with an approximately constant mean, while the stable ones perform a regular relaxation oscillation. In the configuration space it should give the apparent subtle connection shown in Fig. 15.

When the parameter values used are those of the dye laser, $\gamma = 0.5, \sigma = 0.3, \Delta = 0.3, r = 40, g = 0.1$, there persists a very fast relaxation oscillation with frequency $\nu \simeq 3$ which, taking a $\gamma_\perp$ value around 10^9 s^{-1}, gives a period around 1 ns which is typical of the relaxation frequency in dye lasers [58].

It is interesting to point out how in [50] a very similar behavior was found for the array of coupled semiconductor lasers. There the global intensity was more fluctuating because of the smaller number of laser oscillators (2×10), but the switching characteristics are the same.

V. CONCLUSIONS

The most important conclusion is the experimental evidence for turbulent behavior in the laser together with the statement of a model which presents a dynamics closely resembling that observed in the experiments. Our analysis of the experimental results allows us to state that the turbulence is probably weak. The physical relevance of the assumptions held in the statement of the model equations must not be underestimated. In particular, the feasible existence of filamentary structures as dynamical units in these laser systems should be clarified from an analysis based on the full set of partial differential equations. However, both the previous results on filamentary structures and the agreement between the present results and the experiment are cumulative indications that such structures (or something similar to them) exist. The good matching between the dynamical behavior of the model and the experiment (concerning, for example, the frequency locking) indicates that the weak turbulent description is appropriate for the experimental system under study.

To apply the results reported here to concrete laser systems and to be able to predict the appearance of local chaotic behavior, a deeper insight into the mechanism generating the domains is necessary. Once they are clarified, implying some predictive power on the value of the coupling constant g and on the number of domains N, the DMBE's would be a useful tool for studying such systems.

Further experimental work would be useful. For ex-

ample, an analysis of the local dynamics of different laser systems with different lasing substances (such as different dyes in dye lasers) would probably provide an experimental variation of the g value.

From the mathematical viewpoint, one interesting result is the special kind of frequency locking found here. Locking is a very common phenomenon although a complete explanation of the phenomenon has not been found (though studies clarifying some points have been made [57]). Usually a set of oscillators with different natural frequencies lock to a common frequency, often related to those in existence. The interesting aspect of the frequency locking reported here is the fact that the locking frequency is apparently independent of the natural frequencies of the oscillators. Further investigations are necessary to clarify the stabilization mechanism for the frequency at its actual values.

ACKNOWLEDGMENTS

We want to thank Rosa Weigand (Departamento de Optica, Universidad Complutense de Madrid) for her help in the use of the VAX9000 computer on which part of the numerical simulations were done. We are also grateful to J.L. Escudero and I. Gonzalo (Departamento de Optica, Universidad Complutense) and especially to J.R. Tredicce (Institute nonlinearie, Université de Nice) and F.T. Arecchi (Istituto Nazionale di Ottica, Firenze) for discussions. This work has been partially supported by the "Plan General de Promoción del Conocimiento" under Project No. PB92-0798.

APPENDIX A

To prove that the solutions of the DMBE's are bounded, let us make a new change in variables: $x \mapsto x, y \mapsto y, z \mapsto z - r - \sigma$, the equations then being in the form

$$\dot{x}_{ij} = \sigma(y_{ij} - x_{ij}) + ig(\, x_{i+1j} + x_{i-1j} + x_{ij-1} + x_{ij+1} - 4x_{ij}) \,,$$

$$\dot{y}_{ij} = -(1 + i\Delta)y_{ij} - x_{ij}z_{ij} - \sigma x_{ij} \,, \tag{A1}$$

$$\dot{z}_{ij} = -\gamma z_{ij} + \frac{1}{2}(x_{ij}y^*_{ij} + x^*_{ij}y_{ij}) - \gamma(r + \sigma).$$

Let H be the phase space of the system with the Euclidean norm and let $u \in H$. Thus the following equality is straightforward:

$$\frac{1}{2}\frac{d}{dt} \mid u \mid^2 + \sum_{i,j} \left(\sigma \mid x_{ij} \mid^2 + \mid y_{ij} \mid^2 + \gamma z_{ij}^2\right) = -\sum_{i,j} \gamma(r + \sigma) z_{ij} \,. \tag{A2}$$

To obtain this result it is essential that

$$\sum_{i,j} \{x^*_{ij}\,(x_{i+1j} + x_{i-1j} + x_{ij-1} + x_{ij+1} - 4x_{ij}) - x_{ij}\left(x^*_{i+1j} + x^*_{i-1j} + x^*_{ij-1} + x^*_{ij+1} - 4x^*_{ij}\right)\}$$

vanishes, because it contains all the terms $x_{ij}x^*_{i+1j}$ twice and with opposite signs.

We will make use now of the inequality

$$-2\gamma(r + \sigma)z_{ij} \leq \alpha^2 z_{ij}^2 + \frac{\gamma^2}{\alpha^2}(r + \sigma)^2 \,, \tag{A3}$$

α being any real number satisfying $\frac{\alpha^2}{2} < \gamma$. The temporal variation of the norm verifies

$$\frac{d}{dt} \mid u \mid^2 + 2l \mid u \mid^2 \leq \frac{\gamma^2}{\alpha^2}(r + \sigma)^2 N^2 \,, \tag{A4}$$

with $l = \min(1, \sigma, \gamma - \alpha^2) > 0$.

Then, the following upper bound is valid for all time:

$$\mid u(t) \mid^2 \leq |u(0)|^2 e^{-2lt} + \frac{N^2\gamma^2}{2l\alpha^2}(r + \sigma)^2(1 - e^{-2lt}) \tag{A5}$$

and obviously

$$\limsup_{t\to\infty} \mid u(t) \mid \leq \rho_0, \ \rho_0 = \frac{N\gamma(r + \sigma)}{\alpha\sqrt{2l}} \tag{A6}$$

as we wanted to prove.

APPENDIX B

Our first task will be to determine what the lasing solution of (4)–(6) will be and to analyze its stability. We will be mainly interested in the homogeneous solution for physical reasons we will point out later, however, for the sake of generality we will consider the following family of transverse traveling wave solutions (TTWS) with wave number (s, t):

$$F^{st}_{mn} = F^{st}_0 e^{i\left(\frac{2\pi sm}{N} + \frac{2\pi tn}{N}\right)} e^{i\omega^{st}t} \quad P^{st}_{mn} = P^{st}_0 e^{i\left(\frac{2\pi sm}{N} + \frac{2\pi tn}{N}\right)} e^{i\omega^{st}t} D_{mn} = D^{st}_0. \tag{B1}$$

The periodic boundary conditions require the $\mathbf{k}$ values to be of the form $k_x = \pi s$, $k_y = \pi t$, with s, t integers, which has already been used in the previous formulas. Inserting (B1) in the evolution equations, the values of $F^{st}_0, P^{st}_0, D^{st}_0$, and ω^{st} are fixed. The value for the frequency will be used later and is

$$\omega^{st} = -\frac{\sigma\Delta + \alpha^{st}}{\sigma + 1} \,, \tag{B2}$$

where $\alpha_{st} = 4g\left[\sin^2\left(\frac{\pi s}{N}\right) + \sin^2\left(\frac{\pi t}{N}\right)\right]$.

Using the same procedure as Jacobsen *et al.* in Ref. [45] it is found that the traveling wave $\{st\} \equiv (F^{st}_{mn}, P^{st}_{mn}, D^{st}_{mn})$ with the lower threshold is that minimizing Q

$$Q \equiv \min_{s,t}\left\{4g\left[\sin^2\left(\frac{\pi s}{N}\right) + \sin^2\left(\frac{\pi t}{N}\right)\right] - \Delta\right\} \,, \tag{B3}$$

provided the detuning Δ is greater than zero. If $\Delta > 0$ then the homogeneous solution is the more favored one. If g is moderately high and/or the detuning is very small, as is expected in dye lasers, the lower threshold solution will be the homogeneous one $s = t = 0$. In Ref. [45] it was shown for the continuous equation that the solution with the lower threshold also has the greater gain so that its stability in the first lasing state is to be expected.

Depending on the values of the parameters Δ and g one or the other solution will be favored. We have observed (numerically) stable traveling wave solutions in some cases. However, despite being true laser solutions of our lattice with periodic boundary conditions the interest of the TTWS is very limited for many reasons. In the first place, under more physical boundary conditions such as zero boundary conditions with inhomogeneous pumping profile, the TTWS are not solutions and only the inhomogeneous solution which "follows" the pumping makes sense. This solution is an extension of the homogeneous one to space-dependent gain (just change r by r_{ij} in the homogeneous solution) and has nothing to do with traveling waves. Additionally, in the cases of physical interest there is never a perfect symmetry and the traveling waves are generically very unstable with respect to symmetry changes (in [48] a case is studied for traveling waves in a cylindrically symmetric laser). As it takes little effort to analyze the stability of the TTWS together with that of the homogeneous state, we will maintain for a while the more general case. The stability of the homogeneous state has also been studied in the one-dimensional continuous case in Ref. [18].

Let us consider the family of solutions (B1). If we write the linearized equations around any of these solutions, carrying out the change of variables $\delta F^{st}_{mn} = \delta \tilde{x}^{st}_{mn} e^{i\omega^{st}t}$, $\delta P^{st}_{mn} = \delta \tilde{y}^{st}_{mn} e^{i\omega^{st}t}$, $\delta D^{st}_{mn} = \delta \tilde{z}^{st}_{mn}$ the equations adopt an autonomous form. Changing to new variables in Fourier space $\{\delta\xi^{st}_{kl}, \delta\eta^{st}_{kl}, \delta\zeta^{st}_{kl}\}$ defined as

$$\begin{aligned}
\delta\tilde{x}^{st}_{mn} &= \sum_{k,l=0,N-1} \delta\xi^{st}_{kl} e^{2\pi i(km+ln)/N} , \\
\delta\tilde{y}^{st}_{ij} &= \sum_{k,l=0,N-1} \delta\eta^{st}_{kl} e^{2\pi i(km+ln)/N} , \\
\delta\tilde{z}^{st}_{ij} &= \sum_{k,l=0,N-1} \delta\zeta^{st}_{kl} e^{2\pi i(km+ln)/N} ,
\end{aligned} \tag{B4}$$

the linearized equations become decoupled, their form being

$$\begin{aligned}
\delta\dot{\xi}^{st}_{kl} &= \sigma\delta\eta^{st}_{kl} - (\sigma + i\omega)\delta\xi^{st}_{kl} \\
&\quad -4ig\left[\sin^2\left(\frac{\pi k}{N}\right) + \sin^2\left(\frac{\pi l}{N}\right)\right]\delta\xi^{st}_{kl} ,
\end{aligned} \tag{B5}$$

$$\begin{aligned}
\delta\dot{\eta}^{st}_{kl} &= -(a + i\omega^{st})\delta\eta^{st}_{kl} + \delta\xi^{st}_{kl}\left(r - \frac{|A^{st}|^2}{\gamma}\right) \\
&\quad -A^{st}\delta\zeta^{st}_{kl} ,
\end{aligned} \tag{B6}$$

$$\begin{aligned}
\delta\dot{\zeta}^{st}_{kl} &= -\gamma\delta\zeta^{st}_{kl} + \frac{1}{2}\left[A^{st*}\left(1 - i\frac{\omega^{st}}{\sigma}\right)\delta\xi^{st}_{kl}\right. \\
&\quad \left. + A^{*}\delta\eta_{kl} + \text{H.c.}\right] ,
\end{aligned} \tag{B7}$$

where $a = 1 + i\Delta$. In the following the Fourier space variables will be called linear normal modes although they have nothing to do (in general) with the usual empty-cavity modes. Note that the only difference between two normal modes for a given plane wave (s,t) is the coefficient

$$\alpha_{kl} = 4g\left[\sin^2\left(\frac{\pi k}{N}\right) + \sin^2\left(\frac{\pi l}{N}\right)\right] . \tag{B8}$$

The modes with the same value of α_{kl} (i.e., those with $k = i_1, l = i_2$ and $k = i_2, l = i_1$, $i_1 \neq i_2$) are degenerate from the viewpoint of stability so that there is a maximum of $\frac{N(N-1)}{2}$ different values of α_{kl}. The coefficient matrix of the linearized equation for each mode, whose eigenvalues determine its stability, is (omitting the s,t index)

$$\mathbf{M} = \begin{pmatrix}
-(\sigma T + i\alpha_{kl}) & \sigma & 0 & 0 & 0 \\
P & -L & 0 & 0 & -A \\
0 & 0 & -(\sigma T^{*} - i\alpha_{kl}) & \sigma & 0 \\
0 & 0 & P^{*} & -L^{*} & -A^{*} \\
\frac{1}{2}A^{*}T^{*} & \frac{1}{2}A^{*} & \frac{1}{2}AT & \frac{1}{2}A & -\gamma
\end{pmatrix} , \tag{B9}$$

where $T = 1 + i\frac{\omega}{\sigma}$, $L = a + i\omega$ $P = r - |A|^2/\gamma$.

From now on, we will concentrate on the homogeneous solution for the reasons previously explained (the same analysis will be applicable for the more general case with somewhat more algebra). The characteristic polynomial has degree five so that we cannot explicitly find the roots. For the mode with $k = 0, l = 0$ it is easy to find that there is one zero eigenvalue, the characteristic equation being of fourth order and explicitly solvable. The other two eigenvalues are complex, their real parts being negative (at least for σ reasonably small). The reason is that this case is equivalent to the uncoupled CLE, and thus the results of [54] are valid for the stability of this mode. This zero eigenvalue exists as a consequence of a symmetry not broken by the coupling (the global phase changes), as was stated previously.

An essential property in the analysis of the stability is that the modes with α_{kl} satisfying

$$0 < \alpha_{kl} < \frac{2\sigma\Delta}{\sigma + 1}\left(1 - \frac{r_1}{r}\right) \tag{B10}$$

are unstable. This result is similar to that obtained in Ref. [45] for the one-dimensional continuous equation.

The proof of this proposition can be obtained from the characteristic polynomial in λ, which is

$$\lambda^5 + \{2(\sigma+1)+\gamma\}\lambda^4 + \left\{(\sigma+1)^2+\Delta^2-\frac{4\omega^2}{\sigma}+\gamma(r-r_1)+2\gamma(\sigma+1)+\alpha_{kl}^2+2\alpha_{kl}\omega\right\}\lambda^3$$
$$+\left\{(\gamma+2)(\alpha_{kl}^2+2\alpha_{kl}\omega)+\gamma\sigma(\sigma-1)+\gamma r(1+3\sigma)+\gamma\Delta(5-\sigma)\frac{w}{\sigma+1}\right\}\lambda^2$$
$$+\{2\gamma[\sigma(r-1)(\sigma+1)+\omega\Delta]+\alpha_{kl}\gamma\omega[4+(r-r_1)]+\alpha_{kl}^2[\gamma(r-r_1)+2\gamma+r_1]\}\lambda$$
$$+\{\alpha_{kl}^2\gamma r+2(r-r_1)\alpha_{kl}\gamma\omega\}=0\ . \tag{B11}$$

We will first prove the lower bound, i.e., that for $\alpha > 0$ the mode is unstable no matter how small α is. In doing so, we assume there to be an analytic dependence of the polynomial roots on the coupling constant g. For small g values the only root which may have a positive real part is the real one, since it is zero in the case $g = 0$ assuming there is a smooth dependence on g. Let us call the two complex conjugate roots λ_1 and λ_2 and the real root λ_5. We will use a Taylor expansion of the root λ_5 around its value with $g = 0$.

$$\lambda_5 = \lambda_5^{(0)} + \alpha\lambda_5^{(1)} + O(\alpha^2)\ .$$

Putting this form of the solution into the characteristic polynomial and using the fact that $\lambda_5^{(0)} = 0$ is a solution of the $g = 0$ case we obtain the following relation for the first-order coefficient:

$$2(r-r_1)\gamma\omega + \lambda_5^{(1)}2\gamma\{(r-1)(\sigma+1)\sigma+\Delta\omega\} = 0\ . \tag{B12}$$

And then

$$\lambda_5^{(1)} = \frac{\sigma\Delta(r-r_1)}{(\sigma+1)\{(r-1)(\sigma+1)\sigma+\Delta\omega\}}\ ,\quad r > r_1\ . \tag{B13}$$

Thus $\lambda_5^{(1)} > 0$ unless $(r-1)(\sigma+1)\sigma+\Delta\omega < 0$ but this inequality is equivalent to

$$(r-1)(\sigma+1)^2 < \Delta^2 \tag{B14}$$

and so, in order for $\lambda_5^{(1)}$ to be positive, the following expression must be verified:

$$r > 1+\frac{\Delta^2}{(\sigma+1)^2} \equiv r_1\ . \tag{B15}$$

This in fact happens, and thus for small values of the coupling constant the modes are unstable.

We shall look for the upper bound. The two complex solutions λ_1 and λ_2 and the real one λ_5 satisfy

$$|\lambda_1|^2|\lambda_2|^2\lambda_5 = -\{\alpha_{kl}^2\gamma r + 2(r-r_1)\alpha_{kl}\gamma\omega\}\ , \tag{B16}$$

so that in order for λ_5 to be positive the following must hold:

$$\alpha_{kl}r + 2\omega(r-r_1) < 0\ . \tag{B17}$$

We then find the bound

$$\alpha_{kl} < \frac{2\sigma\Delta}{\sigma+1}\left(1-\frac{r_1}{r}\right) \equiv g_0\ . \tag{B18}$$

For the destabilization of the periodic solution, it is sufficient that one of the modes be unstable. Given a g value, the values for the α_{kl} are given by Eq. (B8). The separation of the coupling constants α of adjacent modes (in the sense of coupling) depends on the number of oscillators N. The existence of a region of positive eigenvalues in the range $\alpha_{kl} \in [0, g_0]$ [from (B10)] ensures that the system is unstable if the number of oscillators exceeds a certain critical value, which will be given by the criterion for instability of the $k = 1, l = 0$ mode (remember that the $k = 0, l = 0$ mode will usually be stable).

$$N > N_c = \frac{\pi}{\arcsin\left(\sqrt{\frac{2\sigma\Delta\left(1-\frac{r_1}{r}\right)}{4g(\sigma+1)}}\right)}\ . \tag{B19}$$

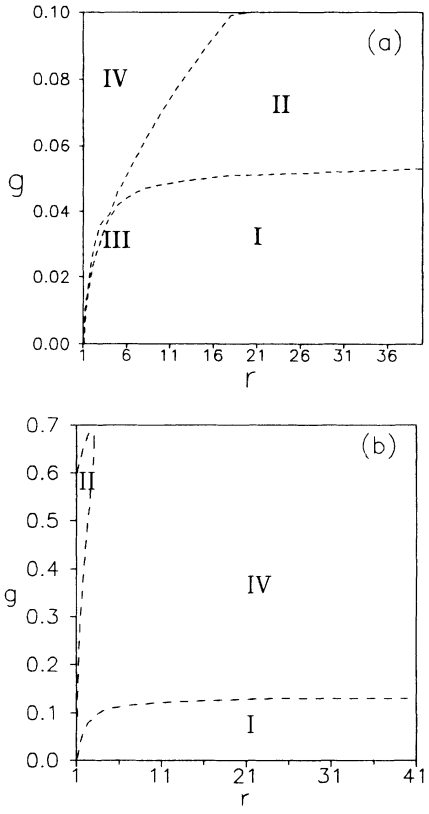

FIG. 16. Stability analysis for some particular cases. (a) $\sigma = 0.1, \gamma = 0.001, \Delta = 0.3$. (b) $\sigma = 0.3, \gamma = 0.1, \Delta = 0.3$. The regions marked with I are those in which the real eigenvalue is positive. The regions marked with II are those in which one of the complex eigenvalues has a positive real part. III means that both the real eigenvalue and one of the complex ones have positive real parts. Finally IV indicates that all eigenvalues have negative real parts (stable states).

This being the more unstable mode (the others having a higher threshold) a number of oscillators below the critical value N_c will imply the stability of the homogeneous state. If the Fresnel number is small the g will take a large value and thus the critical number of oscillators will be quite high. On the contrary, a high Fresnel number will lead to a low coupling constant, and thus to the destabilization of the homogeneous state even when only a few oscillators are present.

Note that the critical number N_c is also dependent on r, so that higher r values increase the instability region, which could be very small near the threshold.

Note that if

$$\frac{2\sigma\Delta}{\sigma+1}\left(1-\frac{r_1}{r}\right) > 4g \tag{B20}$$

then the $k=1, l=0$ mode is unstable no matter what the number of domains is.

Let us introduce some notation. We will call the region of the parameter space where only the real eigenvalue has positive real part "instability region I," the parameter space region in which only a complex eigenvalue has positive real part "instability region II," and the parameter space region in which both a complex eigenvalue and the real one have positive real parts "instability region III." We will say that a mode has "type I instability" if its real eigenvalue is positive, "type II instability" if one of its complex eigenvalues has a positive real part, and "type III instability" if both the real part of one of its complex eigenvalues and its real eigenvalue are positive.

Figure 16 summarizes the stability analysis for some particular parameter values. As stated before, there is always a region for small g values such that positive eigenvalues exist. The equation for the instability frontier between the type I region and the other ones on the g, r plane is given by Eq. (B10), which can be seen in the lower part of the figure. Also included in the figure are other stability and instability regions.

The influence of the number of oscillators is clear from the figures, and the critical number of oscillators can be easily found by inspection. For example, in case (b) a small number of oscillators should imply that only a few α values would stand on the interval $[0, 0.4]$ and thus the first nonzero value of α should be over the region of type I instability, all the modes then being stable (and consequently the limit cycle). An increase in the number of oscillators or a decrease in the value of g would move the lower nonzero value of α towards smaller values, so that it may come into the instability region.

[1] *Hydrodynamic Instabilities and the Transition to Turbulence*, edited by H.W. Swiney and J.P. Gollub, Topics in Applied Physics Vol. 45 (Springer-Verlag, Berlin, 1985).

[2] J.V. Moloney and A.C. Newell, Physica D **44**, 1 (1990).

[3] N.B. Abraham, L.A. Lugiato, and L.M. Narducci, J. Opt. Soc. Am. B **2**, 7 (1985), and other papers in the same issue.

[4] H. Meinhardt, Rep. Prog. Phys. **55**, 797 (1992).

[5] A.M. Turing, Philos. Trans. R. Soc. London, Ser. B **237**, 37 (1952).

[6] I. Prigogine and R. Lefever, J. Chem. Phys. **48**, 1695 (1968); G. Nicolis and I. Prigogine, *Self-Organization Non-Equilibrium Systems* (Wiley, New York, 1974).

[7] For an excellent introduction to these subjects see E. A. Jackson, *Perspectives in Nonlinear Dynamics* (Cambridge University Press, Cambridge, England, 1990), Vol. II, Chap. 10.

[8] H. Haken, *Laser Theory* (Springer-Verlag, Berlin, 1970).

[9] M. Brambilla, F. Battipede, L.A. Lugiato, V. Penna, F. Prati, C. Tamm, and C.O. Weiss, Phys. Rev. A **43**, 5114 (1991).

[10] Yu Anan'ev, *Laser Resonators and the Beam Divergence Problem* (Adam Hilger, Bristol, 1992).

[11] H. Haken, Phys. Lett. **53A**, 77 (1975); for the historical development of the plane-wave approach see N.B. Abraham, L.A. Lugiato, and L.M. Narducci, J. Opt. Soc. Am. B **2**, 7 (1985).

[12] J.D. Gibbon and M.J. McGuiness, Physica D **5**, 108 (1982).

[13] E.N. Lorenz, J. Atmos. Sci. **20**, 130 (1963).

[14] E. Meziane and H. Ladjouze, Phys. Rev. A **44**, 3150 (1991).

[15] D.Y. Tang, M.Y. Li, and C.O. Weiss, Phys. Rev. A **44**, 7597 (1991).

[16] I. Pastor, V.M. Pérez-García, F. Encinas-Sanz, J.M. Guerra, and L. Vázquez, Physica D **66**, 421 (1993).

[17] L.A. Lugiato, G.L. Oppo, M.A. Pernigo, J.R. Tredicce, L.M. Narducci, and D.K. Bandy, Opt. Commun. **68**, 63 (1989); L.A. Lugiato, F. Prati, L.M. Narducci, and G.L. Oppo, *ibid.* **69**, 387 (1989).

[18] L.A. Lugiato, C. Oldano, and L.M. Narducci, J. Opt. Soc. Am. B **5**, 879 (1988).

[19] M. Brambilla, F. Battipede, L.A. Lugiato, V. Penna, F. Prati, C. Tamm, and C.O. Weiss, and Phys. Rev. A **43**, 5090 (1991).

[20] C. Tamm, Phys. Rev. A **38**, 5960 (1988).

[21] I. Iparraguirre and J.M. Guerra, Opt. Commun. **67**, 293 (1988).

[22] W. Klische, C.O. Weiss, and B. Wellegehausen, Phys. Rev. A **39**, 919 (1989).

[23] L.A. Lugiato, G.L. Oppo, L.M. Narducci, J.R. Tredicce, and M.A. Pernigo, J. Opt. Soc. Am. B **7**, 1019 (1990).

[24] J. Tredicce, E.J. Queel, A.M. Gazzawi, C. Green, M.A. Pernigo, L.M. Narducci, and L.A. Lugiato, Phys. Rev. Lett. **62**, 1274 (1989).

[25] L.M. Narducci, G.L. Oppo, J.R. Tredicce, L.A. Lugiato, and F. Prati, in *Coherence and Quantum Optics VI*, edited by J.H. Eberly *et al.* (Plenum Press, New York, 1990).

[26] P. Coullet, L. Gil, and F. Rocca, Opt. Commun. **73**, 403 (1989); P. Coullet, L. Gil, and J. Lega, Physica D **37**, 91 (1989).

[27] F.T. Arecchi, G. Giacomelli, P.L. Ramaza, and S. Residori, Phys. Rev. Lett. **65**, 2531 (1990); **67**, 3749 (1991);

F.T. Arecchi, S. Bocaletti, P.L. Ramaza, and S. Residori, *ibid.* **70**, 2277 (1993).
[28] E. D'Angelo, C. Green, J.R. Tredicce, N.B. Abraham, S 6. Balle, Z. Chen, and G.L. Oppo, Physica D **61**, 6 (1992).
[29] See, for example, the comment on p. 858 in M.C. Cross and P.C. Hohenberg, Rev. Mod. Phys. **65**, 3 (1993).
[30] I. Pastor and J.M. Guerra, Appl. Phys. B **51**, 342 (1990).
[31] I. Pastor, F. Encinas, and J.M. Guerra, Appl. Phys. B **52**, 184 (1991); J.M. Guerra, F. Encinas, and I. Pastor, in *Proceedings of the Third International Workshop on Nonlinear Dynamics and Quantum Phenomena in Optical Systems*, edited by R. Villaseca and R. Corbalán (Springer-Verlag, Berlin, 1990).
[32] D. Dangoisse, D. Hennequin, C. Lepers, E. Louvergnaux, and P. Glorieux, Phys. Rev. A **46**, 5955 (1992).
[33] B.R. Frieden, *Probability, Statistical Optics and Data Testing*, 2nd ed., Springer Series in Information Sciences Vol. 10 (Springer-Verlag, Berlin, 1991).
[34] K. Staliunas, Phys. Rev. A **49**, 1573 (1993).
[35] H. Haken, *Light* (North-Holland, Amsterdam, 1985), Vol. II.
[36] L.A. Lugiato and C. Oldano, Phys. Rev. A **37**, 3896 (1988).
[37] L. Gil, Phys. Rev. Lett. **70**, 162 (1993).
[38] E.A. Jackson and A. Kodogeorgiou, Phys. Lett. A **168**, 270 (1992).
[39] K. Otsuka, Phys. Rev. A **44**, 1393 (1991).
[40] A.G. Cullis, H.C. Weber, and P. Bailey, J. Phys. E **12**, 688 (1979).
[41] S. Diachenko, A.C. Newell, A. Pushkarev, and V.E. Zakharov, Physica D **57**, 96 (1992).
[42] A.C. Newell, Physica D **61**, 213 (1992).
[43] G.L. Oppo and A. Politi, Phys. Rev. A **40**, 1422 (1989).
[44] G.L. Oppo, G. D'Alessandro, and W.J. Firth, Phys. Rev. A **44**, 4712 (1991).
[45] P.K. Jacobsen, J.V. Moloney, A.C. Newell, and R. Indik, Phys. Rev. A **45**, 8129 (1992).
[46] V.I. Emelyanov and V.I. Yukalov, Opt. Spektrosk. **60**, 634 (1986) [Opt. Spectrosc. **60**, 634 (1986)]; A.V. Andreev, V.I. Emelyanov, and Yu.A. Iinskii, *Cooperative Effects in Optics* (IOP Publishing, Bristol, 1992).
[47] See, e.g., M. Born and E. Wolf, *Principles of Optics*, 5th ed. (Pergamon Press, Oxford, 1975).
[48] C. Green, G.B. Midlin, E.J. D'Angelo, H.G. Solari, and J.R. Tredicce, Phys. Rev. Lett. **65**, 3124 (1990); E.J. D'Angelo, E. Izarraguirre, G.B. Mindlin, G. Huyet, L. Gil, and J.R. Tredicce, *ibid.* **68**, 3702 (1992), R. López-Ruiz, G.B. Mindlin, C. Pérez-García, and J. Tredicce, **47**, 500 (1993).
[49] Z. Fei, I. Martín, V.M. Pérez-García, F. Tirado, and L. Vázquez, in *Nonlinear Coherent Structures in Physics and Biology*, Vol. 329 of *NATO Advanced Study Institute, Series B: Physics*, edited by K. H. Spatchek and F. G. Mertens (Plenum Press, New York, 1994); V.M. Pérez-García, J.M. Guerra, and L. Vázquez (unpublished).
[50] R.K. Defreez *et al.*, IEEE Phot. Tech. Lett. **1**, 209 (1989).
[51] R.K. DeFreez *et al.* IEEE Phot. Tech. Lett. **2**, 6 (1990); J. Dong, S. Arai, K. Kudo, and M. Hotta, *ibid.* **5**, 622 (1993).
[52] A. Lapucci and G. Canglioli, Appl. Phys. Lett. **62**, 7 (1993).
[53] K. Otsuka, Phys. Rev. Lett. **65**, 329 (1990).
[54] A.C. Fowler, J.D. Gibbon, M.J. McGuiness, Physica D **4**, 139 (1982).
[55] R. Temam, *Infinite Dimensional Dynamical Systems in Mechanics and Physics*, Applied Mathematical Series Vol. 68 (Springer-Verlag, Berlin, 1988), see Chap. 1, Secs. 1–3.
[56] M. Caponeri and S. Ciliberto, Physica D **58**, 365 (1992).
[57] A.T. Winfree, J. Theor. Biol. **16**, 15 (1967); a recent work with many references is P.C. Mathews, R.E. Mirollo, and S.T. Strogatz, Physica D **52**, 293 (1991); for a system with a few degrees of freedom see, e.g., I. Pastor, V.M. Pérez-García, F. Encinas-Sanz, and J.M. Guerra, Phys. Rev. E **48**, 171 (1993).
[58] Chinlon Lin, IEEE J. Quantum Electron. **11**, 602 (1975); R. Weigand, Ph.D thesis, Universidad Complutense de Madrid, 1993.